crystals

MDPI

Article

Enhancement of Surface and Interface Properties of Low Carbon Steel by Hybrid ZnO and NiO Nanoparticles Reinforced Tin Coating

K. S. Abdel Halim [1,2,*], Mohamed Ramadan [1,2], El-Sayed M. Sherif [3], Khalid M. Hafez [2], Tayyab Subhani [1], Naglaa Fathy [4], Abdulaziz S. Alghamdi [1] and Mohamed H. Khedr [5]

1 College of Engineering, University of Hail, Hail P.O. Box 2440, Saudi Arabia; m.ramadan@uoh.edu.sa (M.R.); ta.subhani@uoh.edu.sa (T.S.); a.alghamdi@uoh.edu.sa (A.S.A.)
2 Central Metallurgical Research and Development Institute (CMRDI), P.O. Box 87, Helwan 11421, Egypt; k.hafez@cmrdi.sci.eg
3 Center of Excellence for Research in Engineering Materials (CEREM), College of Engineering, King Saud University, Riyadh 11421, Saudi Arabia; esherif@ksu.edu.sa
4 Department of Physics, College of Science, University of Hail, Hail P.O. Box 2440, Saudi Arabia; n.ismail@uoh.edu.sa
5 Faculty of Postgraduate Studies for Advanced Sciences, Beni-Suef University, Beni Suef 62521, Egypt; mhkhedr@psas.bsu.edu.eg
* Correspondence: k.abdulhalem@uoh.edu.sa; Tel.: +966-53-145-6640

Abstract: Tin matrix nanocomposite coatings containing ZnO and NiO nanoparticles, both individually and combined, were deposited on low carbon steel substrates. The aim was to investigate the effect of reinforcement of nanoparticles on microstructural morphology and thickness of tin coatings, modification in the interfacial layer between coating and substrate, and the corrosion resistance of low carbon steel substrate. Optical and scanning electron microscopy were employed for microstructural observation, while potentiostat-galvanostat was utilized for electrochemical investigation. It was found that the tin nanocomposite coatings with nanoparticles significantly modified the coating thickness, intermetallic layer thickness, and surface corrosion resistance. Coatings through the direct tinning process are considered to be a simple and low-cost route for protecting metallic materials from corrosion, and the presence of ZnO and NiO nanoparticles in tin coatings further increases the corrosion resistance of low carbon steels.

Keywords: coating; tinning; low carbon steel; interfacial microstructure; corrosion resistance; ZnO; NiO; nanoparticles

check for updates

Citation: Abdel Halim, K.S.; Ramadan, M.; Sherif, E.-S.M.; Hafez, K.M.; Subhani, T.; Fathy, N.; Alghamdi, A.S.; Khedr, M.H. Enhancement of Surface and Interface Properties of Low Carbon Steel by Hybrid ZnO and NiO Nanoparticles Reinforced Tin Coating. *Crystals* **2022**, *12*, 332. https://doi.org/10.3390/cryst12030332

Academic Editor: Shujun Zhang

Received: 24 January 2022
Accepted: 25 February 2022
Published: 27 February 2022

Publisher's Note: MDPI stays neutral with regard to jurisdictional claims in published maps and institutional affiliations.

Copyright: © 2022 by the authors. Licensee MDPI, Basel, Switzerland. This article is an open access article distributed under the terms and conditions of the Creative Commons Attribution (CC BY) license (https://creativecommons.org/licenses/by/4.0/).

1. Introduction

The improvement of surface properties of steel alloys has always been a crucial criterion for their use in advanced engineering applications such as petrochemical processes, automotive industries, and energy transformation. During the application of these alloys, they are exposed to tough environmental conditions such as high temperatures, humidity, corrosion, and wear. Such a severe surrounding environment leads to the corrosion of these materials in shorter times. The corrosion effects always minimize the lifetime, functionality, and safety of these metallic materials. Corrosion is considered one of the most occurring problems in metallic industrial equipment which affects the service life of the equipment and increases the service and maintenance cost. For example, in the automotive industry, corrosion problems are always found at heat sinks, pistons, engine bearings, hose couplings, gear assemblies, carburetors, fuel injectors, shock absorbers, and exhaust system components [1].

Surface modifications of steel alloys offer an attractive solution to combat the damaging effects of corrosion. Surface modifications of metallic alloys were investigated via

different techniques including gaseous, solutions and molten or semi-molten states using hot-dipping, thermal diffusion, thermal spraying, packing, and oxidation processes [2–7]. In these techniques, the selection of the composition of the coated materials is one of the main factors which determine the success of the coating process. Recently, tin (Sn) is becoming the key element in the compositional design of most metallic coating materials which improve the corrosion and oxidation resistance, conductivity, and wear property of metallic substrates [8–10]. The hot-dipped tinning and electrotinning processes are now recommended for many engineering applications due to their cost-effectiveness and ease of controlling and optimizing. In electronics industries, the hot-dipped tinning process has gained wide applications ranging from electronic connectors, lead frames, and integrated circuit plates to current collectors [11]. The use of tin was found to greatly improve the oxidation resistance, conductivity, and wear-resisting properties of substrates [12,13].

One of the most important challenges during tinning of metallic substrates is the phase transformation at coating/substrate interface and the formation of intermetallic compounds (IMCs) which greatly reduce the adhesive strength and the formation of a mechanical bond between coatings and substrates. In order to perform an effective tinning process, the composition, morphology, and thickness of the tin coated layer over the metallic substrates should be adjusted and optimized. The addition of microalloying elements and/or nanoparticles may be a good solution to control the morphology and interface characteristics of the tin coating layer.

Previously the microstructures changes and phase constitutions of the coated layer during the coating process were investigated together with measuring the thicknesses of the intermetallic layers in order to clarify the interaction between mild steel and coated layer [14–23]. It was found that the addition of some alloying particles such as Si, Zn, Cr, Al_2O_3, and others to the coated layer improves the mechanical properties and durability of the coated steel. This can be attributed to the decrease in the thickness of the undesirable intermetallic compound layer that makes the interface between the intermetallic compound layer and substrate smooth and uniform.

Authors of the present work in their previous investigations have handled the direct tinning process over the steel substrates from different viewpoints [24–29]. Especially the effect of process parameters on the interfacial microstructural changes was studied in detail. In a specific study [28], the effect of the addition of alumina nanoparticles to tin coating layer during tinning process on the interfacial microstructure and corrosion behavior of mild steel was investigated. It was found that the presence of alumina nanoparticles in the coating layer improved the surface properties of mild steel substrates. The tin composite coating layer with a relatively high quantity of alumina nanoparticles exhibited better corrosion resistance than other coated layers without nanoparticles. It was concluded that a coating layer with 0.50 wt.% alumina nanoparticles is highly recommended for achieving better corrosion resistance for coated mild steel with minimal coating layer defects.

Accordingly, the present work develops a promising solution for the modification of surface properties of low carbon steels through direct tinning processes using tin nanocomposite reinforced with nano-sized particles of NiO and/or ZnO. It's well known that NiO is highly resistant to corrosion, while ZnO is a multifunctional material due to its exceptional physiochemical properties and broad usefulness [30,31]. It is expected that the presence of these nanoparticles in the tin coated layer will greatly enhance the surface properties and consequently increase their lifetime and protect them from corrosion. The interfacial microstructure of the produced coated materials together with the corrosion behavior was investigated for different compositions of tin coated layers.

2. Experimental

2.1. Synthesis of Nanoparticles

Two kinds of nanoparticles, i.e., ZnO and NiO, were used in the present investigation. The nano-sized NiO powder was prepared through the thermal decomposition of nickel acetate $Ni((CH_3COO)_2{\cdot}4H_2O)$ (WINLAB with assay 98%) at 500 °C for 2 h in a muffle

furnace (DMF-12 Humanlab Instrument Company, Seoul, Korea). The size of the obtained NiO powder was reduced to nanoscale through the ball milling process (Photon Ball Mill, Photon Scientific Company, Qalyub, Egypt) for 1 h at 600 rpm [32]. The nano-sized of ZnO was synthesized using the well-known up-down approach [33]. Briefly, pure ZnO powder (Adwic with assay 98%) was used as the starting material and milled at 600 rpm for 24 h in a stainless-steel vial under atmospheric pressure and room temperature using stainless steel balls. The ball to powder ratio was 10:1. Very fine nano powder with few nanometers was obtained after milling.

2.2. Coating Process

Low carbon steel specimens as shown in Table 1 of approximately 35 × 35 × 5 mm^3 were cut from a long steel sheet and used as substrates in the present study; the chemical composition is given in Table 2. The specimens were ground with emery papers of up to 400 grit size. The specimens were coated by Sn-metal reinforced with nanoparticles of ZnO (0.25 wt.%), NiO (0.25 wt.%), and ZnO/NiO mixture (0.25 wt.% each) through direct tinning technique [28]. The tinning process was performed on steel substrates using tin powder (with and without nanoparticles) mixed with a flux. The flux constituents were: 24 g $ZnCl_2$, 6 g NaCl, 3 g NH_4Cl, 1 mL HCl and 1 mL H_2O. 1 g of pure Sn powder was mixed with 10 g of flux and the estimated ratio of nanoparticles (0.25 wt.%). A layer of the mixture amounting to 0.2 g/cm^2 was distributed on the steel surface area (35 mm × 35 mm). The coated steel substrates were subsequently heated on a hotplate for 2.5 min at 350 °C. After the tinning process, the steel substrates were cooled to room temperature and washed with warm water to remove the remaining flux from the surface of tin layer. The cross-sectional surfaces of the coated specimens (S0–S4) were ground with emery papers of up to 1200 grit size and etched with nital (4% HNO_3 in ethyl alcohol) for microstructural observation.

Table 1. Definitions of the low carbon steel substrate, wt.%.

Sample	Definitions
Sample 0 (S0)	Low carbon steel (LCS)
Sample 1 (S1)	LCS + Sn coating
Sample 2 (S2)	LCS + Sn coating + 0.25 ZnO nanoparticles
Sample 3 (S3)	LCS + Sn coating + 0.25 NiO nanoparticles
Sample 4 (S4)	LCS + Sn coating + (0.25 ZnO + 0.25 NiO) nanoparticles

Table 2. Chemical composition of low carbon steel substrate, wt.%.

Chemical Composition	C	Si	Mn	Cu	Cr	Ni	Al	Fe
Steel substrate	0.08	0.01	0.33	0.03	0.02	0.05	0.05	Bal.

2.3. Microstructural Characterization

Optical and scanning electron microscopes (Field Emission Scanning Electron Microscope, Zeiss Sigma, Oberkochen, Germany) were used to investigate the surface morphology and the microstructures of the coatings and interfaces. The chemical compositions of the interfaces of the coated layer were analyzed using energy-dispersive X-ray spectroscopy (EDS) (Zeiss Sigma, Oberkochen, Germany). The thickness of the surface layers was measured using the Image Analyzer Software (Olympus GX51, Tokyo, Japan). The average thickness of layers was obtained for each sample after measuring at different areas. The phases and crystal size of the prepared nanoparticles were investigated using X-ray diffraction (XRD, PANalytical Empyrean, Eindhoven, The The Netherlands) using CuKα radiation at an accelerating voltage of 40 kV and a current of 35 mA at a wavelength of

λ = 1.54045 Å. The microstructures and morphologies of the nano-sized particles were determined by high-resolution transmission electron microscopy (HRTEM, JEM2100, Jeol, Tokyo, Japan), operated at an acceleration voltage of 200 kV.

2.4. Corrosion Test

For electrochemical measurements, a three electrodes electrochemical cell (PGSTAT-302N Autolab Potentiostat-Galvanostat) (Metrohm, Amsterdam, The Netherlands) that accommodates for 0.200 L solution was employed. The test samples served as the working electrode, a silver-silver chloride (Ag/AgCl in saturated KCl solution) (Metrohm, Amsterdam, The Netherlands) was the reference electrode, and a Pt sheet was the counter electrode. The potentiodynamic cyclic polarization (PCP) data was obtained between −1.2 V and 0.0 V at a 0.00167 V/s scan rate. The electrochemical impedance spectroscopy (EIS) plots were collected from the values of the open circuit potential (OCP) for a frequency scan range between 100,000 Hz and 0.1 Hz at an AC wave of 5 mV peak-to-peak overlaid.

3. Results and Discussion

3.1. Characterization of the Starting Materials

The microstructure of low carbon steel substrate (S0) is shown in Figure 1; the common phases of ferrites and pearlites can be observed. The percentage of the two phases is mainly verified by the lower carbon percentage of the steel substrate. The amounts of the two phases in microstructure verify the carbon percentage present in low carbon steel.

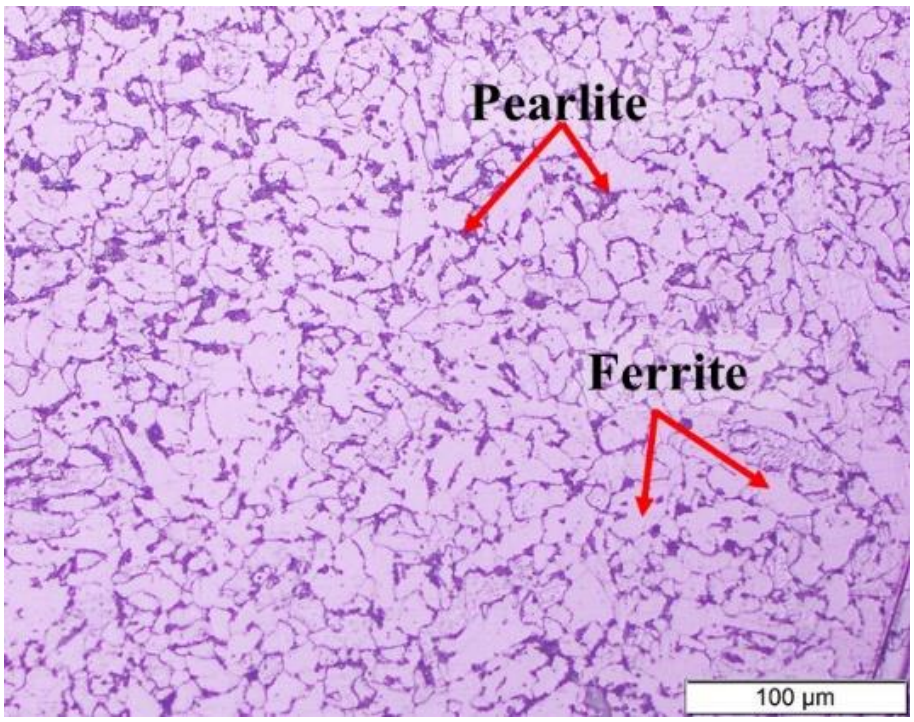


Figure 1. Microstructure of carbon steel (S0).

The SEM-TEM images and XRD patterns of the as-prepared particles are shown in Figures 2 and 3, respectively. The SEM images and the particles size investigations for multi-areas of ZnO and NiO specimens (obtained from SEM images and image analyzer measurements) showed that the as-prepared ZnO particles were in both rod and spherical shapes with average particles size of about 95 ± 10 nm. However, the as-prepared NiO specimen showed spherical shapes with average particles size of about 60 ± 7 nm.

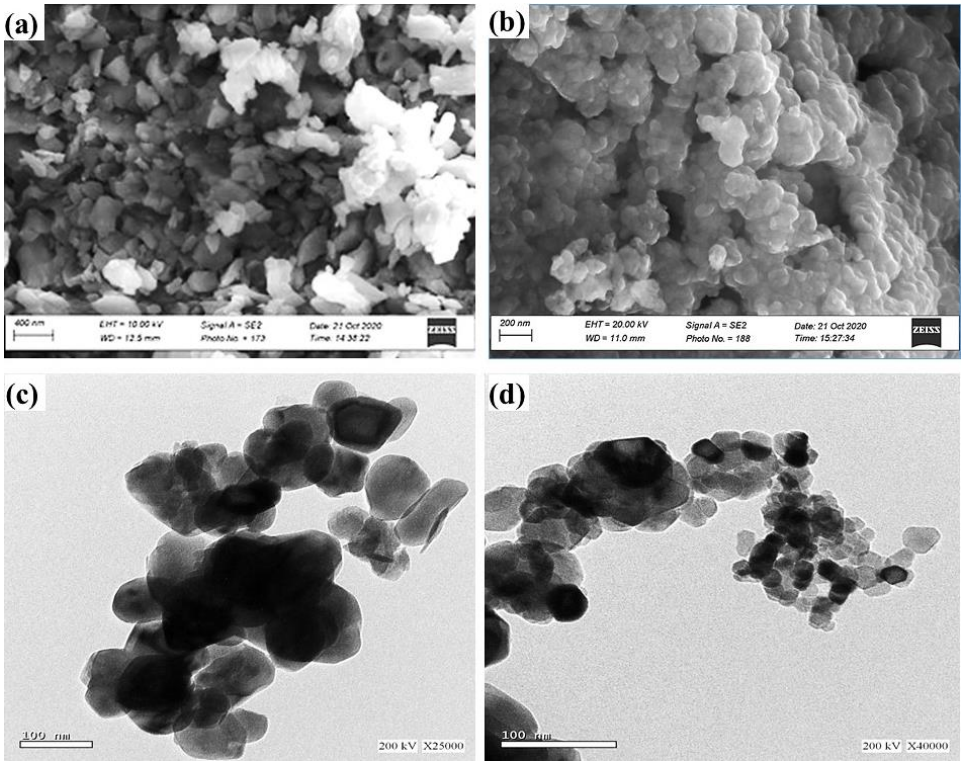


Figure 2. SEM and TEM images of nano-sized particles of; (**a**,**c**) ZnO (**b**,**d**) NiO.

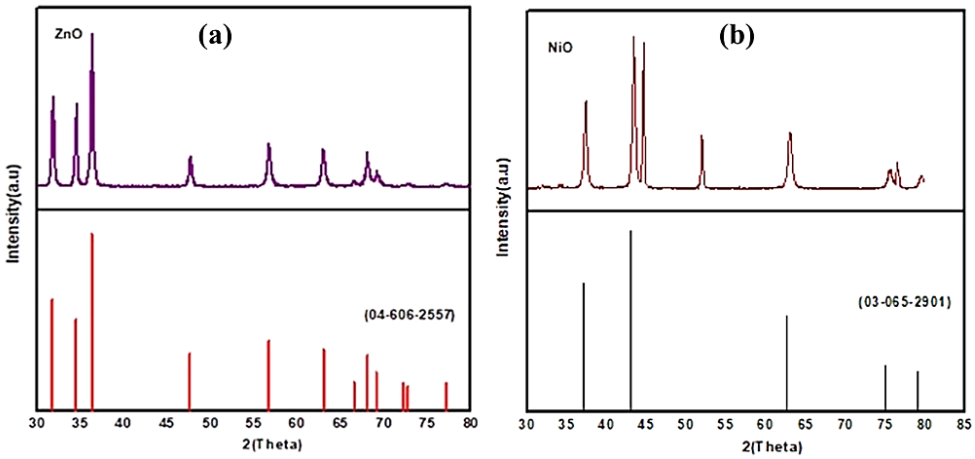


Figure 3. XRD analysis of nano-sized particles of; (**a**) ZnO (**b**) NiO.

3.2. Microstructural Changes Accompanying Tinning Process

The cross-sectional microstructures of low carbon steel substrates with tin coating and tin-nanocomposite coatings containing ZnO and/or NiO nanoparticles are presented in Figure 4. It can be observed that the morphology of the coating layer plays an important role in the formation and nature of the intermetallic layer of Sn-composites coatings. Furthermore, the thickness of surface and intermetallic layers of tin-composites coating layers are highly affected by the presence of reinforced nanoparticles materials. The low carbon steel substrate coated only with tin (without nanoparticles addition) shows an irregular and very thin coated layer with a minimum thickness (Figure 4a). However, the presence of ZnO nanoparticles in the coating layer (Figure 4b) shows and relatively thick coated layer. It is interesting to observe that the presence of NiO nanoparticles in the coating layer (Figure 4c) has a different effect on the thickness of the interfacial layer, where it hinders the increase of the thickness of the interfacial layer. A remarkable change in the

coated layer is observed when using mixed oxides of ZnO + NiO nanoparticles as it greatly increases the thickness of the interfacial layer of coating materials.

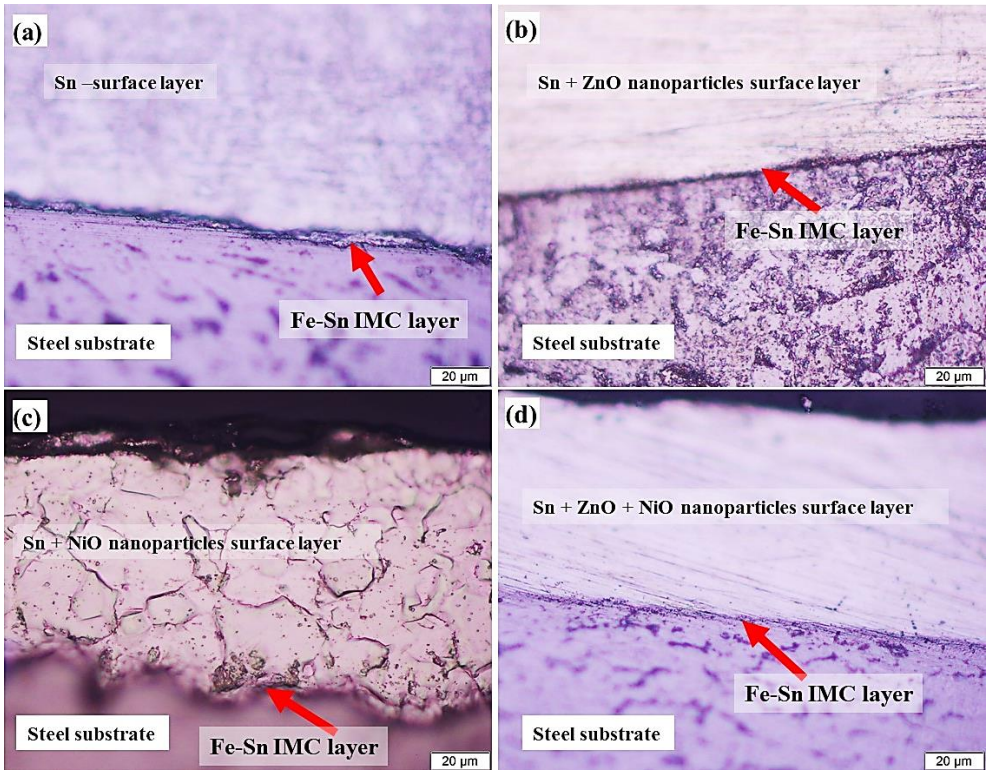


Figure 4. Microstructures of four different coating surfaces and interfacial layers of steel, (**a**) Pure Sn coating (S1), (**b**) Sn+ ZnO nanoparticles coating (S2), (**c**) Sn+ NiO nanoparticles coating (S3), (**d**) Sn + ZnO + NiO nanoparticles coating (S4).

The SEM image of a cross-section of low carbon steel substrate coating with tin without any addition of nanoparticles (S1 substrate) is shown in Figure 5 alongside the presentation of an EDS microanalysis. The typical microstructure of a tin coating layer at the Fe-Sn intermetallic interface and typical ferrite-pearlite can be observed. The EDS pattern in the tin coating surface layer near the coating surface was analyzed. The green axis represents the line scan distance and elements intensities. The pattern of tin coating surface layer adjacent to interface layer displays Fe element due to diffusion from higher concentrations of iron and low carbon steel to Sn-coating. A clear interface between the tin coating surface layer and low carbon steel indicates the presence of intermetallic compound (IMCs) (Fe-Sn intermetallic phase) due to the reaction of tin with iron. The evolution and growth of IMCs play an important role in the mechanical properties and reliability of the coating layer. A detailed analysis of the thickness of both the interfacial layer and intermetallic layer is shown in Figures 6 and 7, respectively. The maximum coating thickness of 69.61 $\pm$ 2 µm was achieved for hybrid ZnO and NiO nanoparticles in the tin coating It is clear that the addition of nanoparticles resulted in an increase in the wetting area and an increase in the microhardness of the coating materials [28]. The regularity of tin-composites coating layers is improved due to the improvement in wettability between the coating layer and the steel.

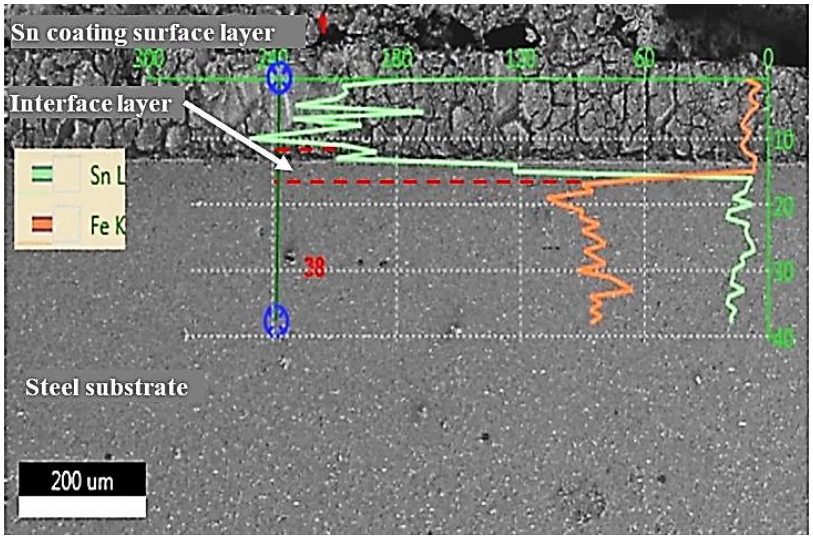


Figure 5. SEM photograph and EDS line scan across Sn coating layer and steel substrate (S1).

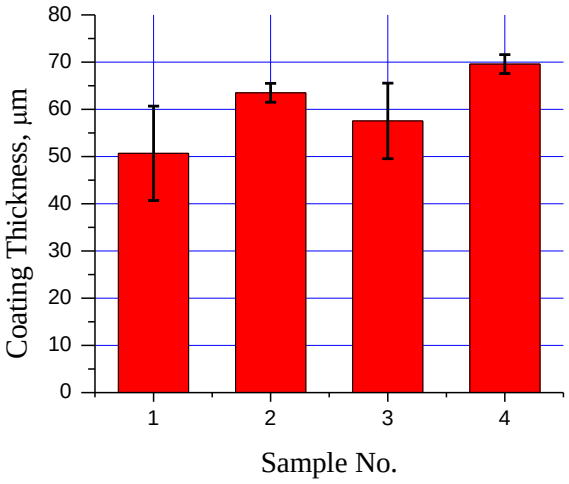


Figure 6. Coating thicknesses of four different coating surfaces and interfacial layers of steel, (**1**) Pure Sn coating (S1), (**2**) Sn + ZnO nanoparticles coating (S2), (**3**) Sn + NiO nanoparticles coating (S3), (**4**) Sn + ZnO + NiO nanoparticles coating (S4).

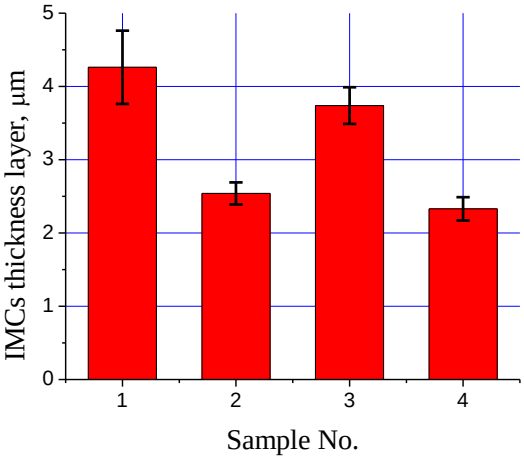


Figure 7. IMCs thicknesses of four different coating surfaces and interfacial layers of steel, (**1**) Pure Sn coating (S1), (**2**) Sn + ZnO nanoparticles coating (S2), (**3**) Sn + NiO nanoparticles coating (S3), (**4**) Sn + ZnO + NiO nanoparticles coating (S4).

As shown in Figure 7, the effect of nanoparticles addition on the thickness of the tin surface layer and iron-tin IMC interface is very clear and it is enhanced with the presence of ZnO nanoparticles alone or when mixed with NiO nanoparticles. It can be observed that the maximum increase in thickness of the tin surface layer is associated with the presence of ZnO + NiO nanoparticles in the coating layer. This can be attributed to the morphology changes of the surface layer during the tinning process. On the other hand, the maximum decrease in the thickness of the Fe-Sn IMC interface seems to be found in the coating layer containing both ZnO and NiO nanoparticles (S4). A minimum coating thickness of about 2.33 ± 0.16 µm was observed in the IMC layer for hybrid ZnO and NiO nanoparticles in the tin coating which means a remarkable decrease in the thickness of the IMC interface is observed in the S4 substrate.

3.3. Corrosion Resistance Enhancement

3.3.1. Potentiodynamic Cyclic Polarization Measurements

PCP curves obtained for different samples after 1 h immersion in 3.5% NaCl solutions are depicted in Figure 8 while the corrosion data is summarized in Table 3. βc and βa are the cathodic and anodic Tafel slopes, respectively, and E_{Corr}, j_{Corr}, R_P, and R_{Corr} are the corrosion potential, corrosion current density, polarization resistance, and corrosion current. The values of βc, βa, E_{Corr}, and j_{Corr} were obtained, as reported in the previous work [34–36]. Moreover, the values of both R_P and R_{Corr} were calculated according to the following relations [36–39]:

$$R_P = \frac{1}{j_{Corr}} \left(\frac{\beta_c . \beta_a}{2.3(\beta_c + \beta_a)} \right) \quad (1)$$

$$R_{Corr} = j_{Corr} \left(\frac{k . E_W}{d . A} \right) \quad (2)$$

where, k is a constant (to define the unit for R_{Corr}, k = 3272 mm (amp^{-1} cm^{-1} year^{-1})), E_W is the equivalent weight of the mild steel (E_W = 28.25 g equivalent), d is the density of mild steel (d = 7.84 gm cm^{-3}), and A is the area of the surface (A = 1 cm^2).

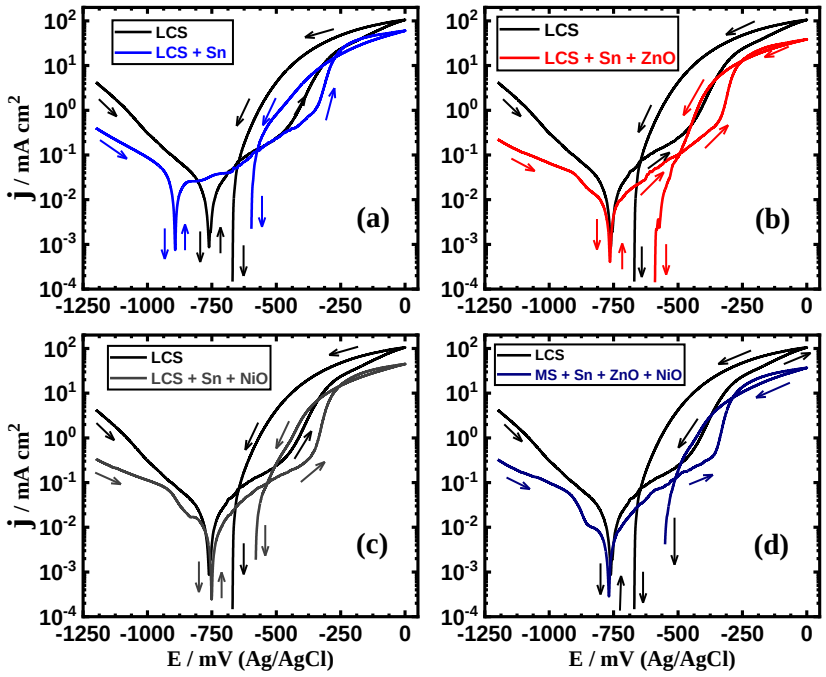


Figure 8. Cyclic potentiodynamic polarization for, (**a**) LCS, LCS + Sn, (**b**) LCS, LCS + Sn + ZnO, (**c**) LCS, LCS + Sn + NiO, and (**d**) LCS, LCS + Sn + ZnO + NiO, samples after 1 h immersion in 3.5% NaCl solution.

Table 3. Corrosion parameters obtained from polarization curves.

Sample	βc (mV/dec)	E_{Corr} (mV)	βa (mV/dec)	j_{Corr} (μA/cm^2)	R_P (kΩ cm^2)	R_{Corr} (mmy^{-1})
Low carbon steel (LCS)	125	−774	180	17.5	1.83	0.2063
LCS + Sn	118	−880	150	14.6	1.97	0.1721
LCS + Sn + ZnO	100	−767	135	0.65	38.43	0.0077
LCS + Sn + NiO	92	−755	122	0.55	41.46	0.0065
LCS + Sn + ZnO + NiO	83	−745	120	0.45	47.40	0.0053

Figure 8 shows that the obtained current of all samples decreases in the cathodic current with sweeping the potential in the cathodic branch. This is due to the oxygen reduction reaction that takes place on the surface of the tested samples as follows [34,35,40]:

$$2H_2O + O_2 + 4e^- \rightarrow 4OH^- \quad (3)$$

The strong this reaction is, the more output current is recorded. From this point of view, the highest values of the cathodic currents are recorded for the low carbon steel sample indicating that the uncoated mild steel has the most active surface. The cathodic current is also seen to decrease with the coating of steel with Sn, Sn + ZnO, Sn + NiO, and Sn + ZnO + NiO. The sample that is coated with Sn + ZnO + NiO has the lowest values of currents.

The anodic current, in turn, shows the highest values for bare sample (S0), where the current of the steel increases at the start of the anodic branch due to the dissolution of the steel surface as follows [34,35,40]:

$$Fe^0 = Fe^{2+} + 2e^- \quad (4)$$

The current continuously increases, showing a slight passive region with the increase of the applied potential. The appearance of the slight passive region may have resulted from the reaction of the iron surface with oxygen from the solution to form $Fe(OH)_2$ and Fe_3O_4 according to the following equations [38];

$$Fe^0 + \frac{1}{2} O_2 + H_2O \rightarrow Fe(OH)_2 \quad (5)$$

$$3Fe(OH)_2 + \frac{1}{2} O_2 \rightarrow Fe_3O_4 + 3H_2O \quad (6)$$

The anodic current of the LCS sample abruptly increased with the continuous sweeping of potential in the positive direction in the presence of the chloride ions due to the breakdown of the formed oxide film (Equations (5) and (6)). The continues increase in current is due to the occurrence of pitting corrosion under the chloride ions attach to the surface and the high anodic potential as follows [35];

$$Fe_{(s)} + 2Cl^-_{(aq)} = FeCl_{2(s)} + 2e^- \quad (7)$$

$FeCl_2$ transfers from the surface to the interface and again to the solution (8):

$$FeCl_{2(s)} = FeCl_{2(interface)} \rightarrow FeCl_{2(aq)} \quad (8)$$

The occurrence of pitting corrosion for the LCS sample at this condition was also confirmed by the appearance of a hysteresis loop, where the obtained current in the backward direction was higher than the current obtained from the forward direction.

On the other hand, the anodic currents for all coated samples show an active-passive behavior, where the current abruptly increases only at the start of the anodic branch then shows a passive layer that is an oxide film of the coating layer. The coating layer as well as the formed oxide(s) are compact and lead to protecting the surface of the sample from dissolution at certain potential values. Further applying the anodic potential in the presence of the corrosive chloride solution leads to an abrupt increase in the current values due to

the dissolution of the formed layers on the surface of the samples. Reversing the scanned potential in the backward direction zero to ~ −300 mV resulted in a smaller current as compared to the obtained currents in the forward direction. This behavior for all coated steel samples proves that the pitting corrosion does not occur at these conditions. It is to be mentioned here that the presence of Sn coating provides protection to LCS, and this effect increased after the addition of 0.25% ZnO nanoparticles and still more with NiO nanoparticles; while the highest impact of reducing the corrosion was recognized after the addition of both ZnO and NiO nanoparticles to the coated Sn low steel sample.

3.3.2. Electrochemical Impedance Spectroscopy Measurements

EIS measurements were carried out in order to confirm the data obtained from the PCP experiments. The EIS method can be successfully employed to report the corrosion and corrosion protection for metallic materials in numerous corrosive media [38–41]. The Nyquist plots were collected for LCS, LCS + Sn, LCS + Sn + ZnO, LCS + Sn + NiO, and LCS + Sn + ZnO + NiO samples after their immersion for 1 h in 3.5% NaCl solution. The measured impedance data were fitted to the best equivalent circuit model that is depicted in Figure 9. The definition of the symbols presented in the equivalent circuit is defined in the caption of Figure 9; the values of these parameters were collected and recorded in Table 4. The first polarization resistance, R_{P1}, can be considered as the resistance at the interface between samples' surface and the corrosion product or the coating layer, while the second polarization resistance, R_{P2}, expresses corrosion resistance for the interface between the top layer formed on the samples and the solution.

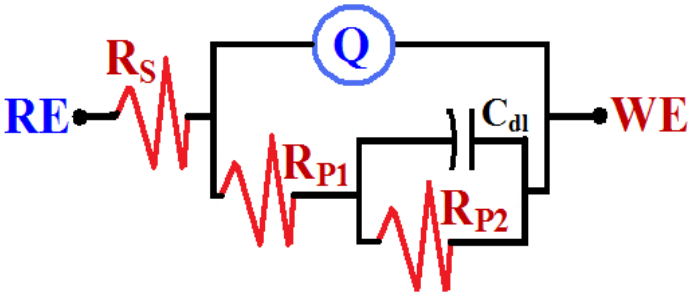


Figure 9. Equivalent circuit model with its elements defined as; reference electrode (RE), solution resistance (R_S), constant phase elements (Q, CPEs), first polarization resistance (R_{P1}), double layer capacitance (Cdl), second polarization resistance (R_{P2}), and the working electrode (WE).

Table 4. Parameters obtained from fitting the impedance data.

Sample	R_S/ Ω cm^2	Q		R_{P1}/ Ω cm^2	C_{dl}/ μF cm^{-2}	R_{P2}/ Ω cm^2
		Y_Q/F cm^{-2}	n			
Low carbon steel (LCS)	2.799	0.004096	0.67	24.54	0.606	172.1
LCS + Sn coating	3.814	0.002401	0.80	29.97	0.355	255.8
LCS + Sn + ZnO	4.333	0.001905	0.75	31.29	0.250	376.9
LCS + Sn + NiO	5.503	0.001085	0.72	35.18	0.177	577.6
LCS + Sn + ZnO + NiO	6.645	0.000936	0.80	39.88	0.107	721.5

As shown in Figure 10, all spectra show only one semicircle whose diameter is the smallest for the LCS sample. Coating the steel with a tin layer led to increasing the diameter of the semicircle indicating that the corrosion resistance increases in the presence of the tin coated layer. Incorporating 0.25% of the ZnO nanoparticles with the Sn coated layer on the surface of the LCS sample led to a wider semicircle and a slightly higher effect was noticed when 0.25% NiO nanoparticles were added to the tin coating on the surface of LCS. The largest diameter of a semicircle was obtained for the steel sample that had both ZnO and NiO nanoparticles incorporated with the tin coating. The listed parameters in Table 4 confirmed that the values of resistances, R_S, R_{P1}, and R_{P2} increased after adding ZnO and NiO either individually or combined. Also, the presence of Q (with its "n" values were

varied between 0.67 and 0.80) here can be considered as double layer capacitance with some pores to reduce the charged sample surfaces. Moreover, the values of Y_Q and C_{dl} were noticed to decrease in the presence of the tin coating layer, and further decreases were recorded in the presence of ZnO and NiO nanoparticles, where the lowest values were noticed for the LCS + tin + ZnO + NiO sample. The EIS measurements agree with the data obtained from the polarization experiments, and both confirm that coating the steel with tin increases the corrosion resistance in the chloride test solution, and this effect increases by adding ZnO and NiO nanoparticles.

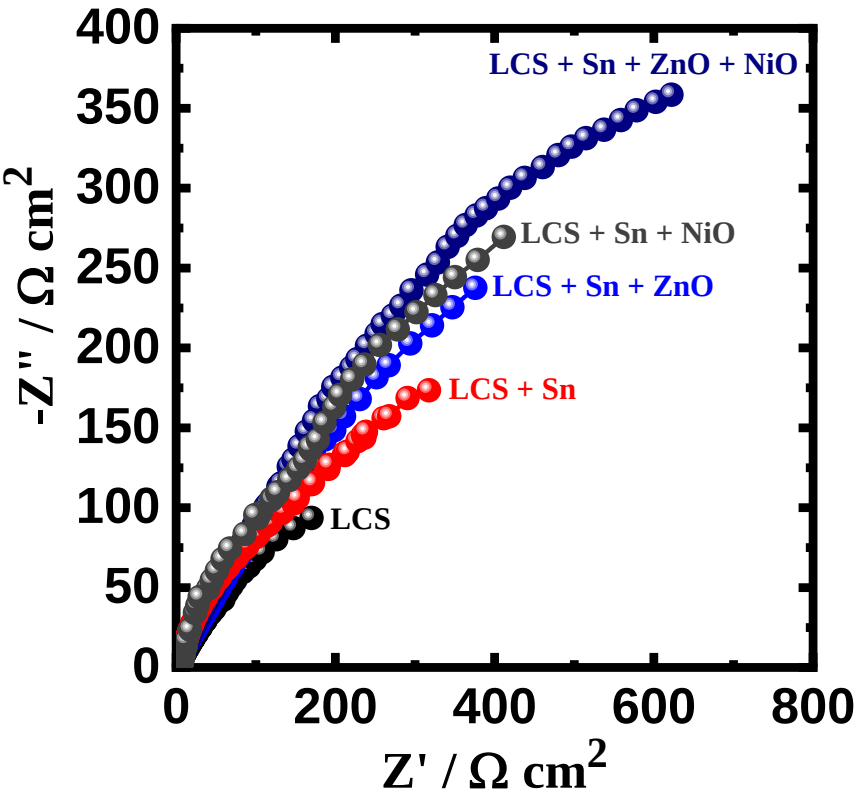


Figure 10. Nyquist plots for LCS, LCS + Sn, LCS + Sn + ZnO, LCS + Sn + NiO, and LCS + Sn + ZnO + NiO samples after 1 h immersion in 3.5% NaCl solution.

4. Conclusions

The influence of tin coating reinforced with ZnO and NiO nanoparticles on corrosion properties and the interfacial layer of low carbon steel were studied. Based on the obtained results, the following conclusions can be pointed out as follow:

1. The uniform coating surface with regular interface structure was achieved by individual ZnO and the combined addition of ZnO and NiO nanoparticles in the tin coating.
2. The tin coating thickness increased with the addition of ZnO, NiO, and hybrid ZnO/NiO nanoparticles. The maximum coating thickness of 69.61 ± 2 µm was achieved for hybrid ZnO and NiO nanoparticles in the tin coating.
3. Fe-tin intermetallic interfacial layer thickness decreased with the addition of ZnO, NiO, and hybrid ZnO/NiO nanoparticles. The minimum coating thickness of about 2.33 ± 0.16 µm was achieved for hybrid ZnO and NiO nanoparticles in the tin coating.
4. Tin coatings which were formed by the addition of ZnO, NiO, and hybrid ZnO/NiO nanoparticles showed improvement in corrosion resistance in comparison with the pure tin coating.
5. The best improvement in corrosion resistance was achieved by using hybrid ZnO/NiO nanoparticles in the tin coating.

Author Contributions: Conceptualization, K.S.A.H. and M.R.; Data curation, K.M.H., A.S.A. and E.-S.M.S.; Formal analysis, E.-S.M.S., N.F. and M.R.; Investigation, K.S.A.H., K.M.H., E.-S.M.S., M.R. and M.H.K.; Methodology, K.S.A.H., T.S., A.S.A., N.F. and M.R.; Project administration, A.S.A. and K.S.A.H.; Software, T.S. and M.H.K.; Writing—review & editing, K.S.A.H., E.-S.M.S., M.R. and T.S. All authors have read and agreed to the published version of the manuscript.

Funding: This research has been funded by Scientific Research Deanship at the University of Ha'il—Saudi Arabia through project number RG- 20 027.

Institutional Review Board Statement: Not applicable.

Informed Consent Statement: Not applicable.

Data Availability Statement: Data available in a publicly accessible.

Conflicts of Interest: The authors declare no conflict of interest.

References

1. Chintada, V.B.; Koona, R.; Raju Bahubalendruni, M.V.A. State of Art Review on Nickel-Based Electroless Coatings and Materials. *J. Bio- Tribo-Corros.* **2021**, *7*, 134. [CrossRef]
2. Holmberg, K.; Matthews, A. Surface coating methods. In *Tribology Series Book*; Elsevier Science: Amsterdam, The Netherlands, 1994; Volume 28, ISBN 9780080875927.
3. Sharma, S.; Agarwala, P.; Garg, R.; Gopinath, P. A study on Ni-P and Ni-P-ZnO composite coatings developed by electroless technique. In *Advanced Materials Research*; Trans Tech Publications Ltd.: Kapellweg, Switzerland, 2012; Volume 585, pp. 512–516.
4. Vitry, V.; Kanta, A.F.; Delaunois, F. Application of nitriding to electroless nickel–boron coatings: Chemical and ctural effects; mechanical characterization; corrosion resistance. *Mater. Des.* **2012**, *39*, 269–278. [CrossRef]
5. Narayanan, T.S.; Krishnaveni, K.; Seshadri, S.K. Electroless Ni–P/Ni–B duplex coatings: Preparation and evaluation of microhardness, wear and corrosion resistance. *Mater. Chem. Phys.* **2003**, *82*, 771–779. [CrossRef]
6. Zhang, W.X.; Jiang, Z.H.; Li, G.Y.; Jiang, Q.; Lian, J.S. Electroless Ni-P/Ni-B duplex coatings for improving the hardness and the corrosion resistance of AZ91D magnesium alloy. *Appl. Surf. Sci.* **2008**, *254*, 4949–4955. [CrossRef]
7. Balaraju, J.N.; Selvi, V.E.; Rajam, K.S. Electrochemical behaviour of low phosphorus electroless Ni–P–Si_3N_4 composite coatings. *Mater. Chem. Phys.* **2010**, *120*, 546–551. [CrossRef]
8. Gines, M.J.L.; Benítez, G.J.; Egli, W.; Zubimendi, J.L.; Pérez, Z.T. Formation of an Fe-Sn Intermetallic Layer During the Reflow Process After Tin Plating. *Plat. Surf. Finish.* **2003**, *90*, 44–49.
9. Wijaya, R.H.; Soegijono, B. Corrosion Resistance of Sn-Zn Coated on Low Carbon Steel Material in Wet Gas Pipeline. *IOP Conf. Ser. Mater. Sci. Eng.* **2019**, *694*, 012029. [CrossRef]
10. Xiang, N.; Yin, T.; Tian, B.; Tang, S.; Chen, E. Evaluation on the Manufacturability of Solderable Sn Coatings Obtained by Employing Hot-Dipped Tinning Process. *JOM Adv. Surf. Eng.* **2019**, *71*, 4284. [CrossRef]
11. Diao, H.; Wang, C.Q.; Wang, L. Bonding of Aluminum Alloy by Hot-Dipping Tin Coating. *Adv. Mater. Res.* **2008**, *32*, 93–98. [CrossRef]
12. Spitz, M.; Fleischanderl, M.; Sierlinger, R.; Reischauerb, M.; Perndorfer, F.; Fafilek, G. Surface lubrication influence on electrode degradation during resistance spot welding of hot dip galvanized steel sheets. *J. Mater. Process. Technol.* **2015**, *216*, 339–347. [CrossRef]
13. Makhatha, M.E.; Fatoba, O.S.; Akinlabi, E.T. Effect of rapid solidification on the microstructure and surface analyses of laser deposited Al-Sn coatings on AISI 1015 steel. *Int. J. Adv. Manuf. Technol.* **2018**, *94*, 773–787. [CrossRef]
14. Morita, J.; Yoshida, M. Chromium coating on partially tin precoated steel sheet. *J. Appl. Electrochem.* **1994**, *24*, 888–893. [CrossRef]
15. Vitkin, A.I.; Surovtseva, V.S. New protective coating in the production of sheet metal. *Metallurg* **1972**, *16*, 286–290. [CrossRef]
16. Zhao, X.; Wen, Y.; Li, Y.; Liu, Y.; Wang, Y. Effect of Fe_2O_3 nanoparticles size on the properties of Sn-1.0Age0.5Cu nano-composite solders and joints. *J. Alloys Compd.* **2016**, *662*, 272–282. [CrossRef]
17. Nejad, M.M.; Habibolahzadeh, A.; Yousefpour, M. Effect of Nano_Oxide Addition on Corrosion Performance of Hot Dip Zinc Coating. *Prot. Met. Phys. Chem. Surf.* **2016**, *52*, 100–103. [CrossRef]
18. Jiang, Z.H.; Han, J.P.; Li, Y. Effect of tin on corrosion resistance and formability of tin bearing ferritic stainless steel. *Mater. Res. Innov.* **2014**, *18*, 9–11. [CrossRef]
19. Awan, G.H.; Ahmed, F.; Ali, L.; Shuja, M.S.; Hasan, F. Effect of coating-thickness on the formability of hot dip aluminized steel. *Pak. J. Engg. Appl. Sci.* **2008**, *2*. Available online: https://www.researchgate.net/publication/241024789_Effect_of_Coating-thickness_on_the_Formability_of_Hot_Dip_Aluminized_Steel (accessed on 1 January 2022).
20. Springer, H.; Kostka, A.; Payton, E.J.; Raabe, D.; Kaysser-Pyzalla, A.; Eggeler, G. On the formation and growth of intermetallic phases during interdiffusion between lowcarbon steel and aluminum alloys. *Acta Mater.* **2011**, *59*, 1586–1600. [CrossRef]
21. Dey, P.P.; Modak, P.; Ghosh, A.; Chakrabarti, D.; Banerjeem, P.S.; Ghosh, M. Investigation of phase evolution of Al–Si–Mg coating on hot dipped interstitial-free steel. *Results Mater.* **2020**, *6*, 100078. [CrossRef]

22. Bahadur, A.; Mohanti, O.N. Aluminium diffusion coating on medium carbon steel. *Mater. Trans. JIM* **1995**, *36*, 1170–1175. [CrossRef]
23. Xiang, Z.D.; Datta, P.K. Relationship between pack chemistry and aluminide coating formation for low-temperature aluminisation of alloy steels. *Acta Mater.* **2006**, *54*, 4453–4463. [CrossRef]
24. Ramadan, M.; Alghamdi, A.S.; Hafez, K.M.; Subhani, T.; Abdel Halim, K.S. Development and Optimization of Tin/Flux Mixture for Direct Tinning and Interfacial Bonding in Aluminum/Steel Bimetallic Compound Casting. *Materials* **2020**, *13*, 5642. [CrossRef] [PubMed]
25. Ramadan, M.; Alghamdi, A.S.; Subhani, T.; Halim, K.S.A. Fabrication and Characterization of Sn-Based Babbitt Alloy Nanocomposite Reinforced with Al_2O_3 Nanoparticles/Carbon Steel Bimetallic Material. *Materials* **2020**, *13*, 2759. [CrossRef] [PubMed]
26. Ramadan, M.; Ayadi, B.; Rajhi, W.; Alghamdi, A.S. Influence of Tinning Material on Interfacial Microstructures and Mechanical Properties of Al12Sn4Si1Cu /Carbon Steel Bimetallic Castings for Bearing Applications. *Key Eng. Mater.* **2020**, *835*, 108–114. [CrossRef]
27. Ramadan, M.; Hafez, K.M.; Alghamdi, A.S.; Ayadi, B.; Abdel Halim, K.S. Novel Approach for Using Ductile Iron as Substrate in Bimetallic Materials for Higher Interfacial Bonding Bearings. *Int. J. Met.* **2021**, 1–14. [CrossRef]
28. Alghamdi, A.S.; Halim, K.S.A.; Amin, A.; Alshammari, S.; Fathy, N.; Ramadan, M. Interfacial Microstructure and Corrosion Behaviour of Mild Steel Coated with Alumina Nanoparticles Doped Tin Composite via Direct Tinning Route. *Coatings* **2021**, *11*, 1318. [CrossRef]
29. Fathy, N.; Ramadan, M. Influence of volume ratio of liquid to solid and low pouring temperature on interface structure of cast Babbitt-steel bimetal composite. *AIP Conf. Proc.* **2018**, *1966*, 20028.
30. Narender, S.S.; Varma, V.S.; Sai Srikar, C.; Ruchitha, J.; Adarsh Varma, P.; Praveen, B.V.S. Nickel Oxide Nanoparticles: A Brief Review of Their Synthesis, Characterization, and Applications. *Chem. Eng. Technol.* **2022**. [CrossRef]
31. Wojnarowicz, J.; Chudoba, T.; Lojkowski, W. A Review of Microwave Synthesis of Zinc Oxide Nanomaterials: Reactants, Process Parameters and Morphologies. *Nanomaterials* **2020**, *10*, 1086. [CrossRef]
32. Balboul, B.A. Surface Active Rubidium Carbonate Obtained from the Thermal Decomposition Course of Rubidium Acetate. *Egypt. J. Chem.* **2012**, *54*, 455–467.
33. Giri, P.K.; Singh, K.D.; Kesavamoorthy, R.; Panigrahi, B.K.; Nair, K.G.M. Correlating the microstructural and photoluminescence properties of ZnO nanoparticles prepared by ball milling. In *2007 International Workshop on Physics of Semiconductor Devices*; IEEE: Piscataway, NJ, USA, 2007; pp. 905–908. [CrossRef]
34. Ahmed, A.H.; Sherif, E.-S.M.; Abdo, H.S.; Gad, E.S. Ethanedihydrazide as a Corrosion Inhibitor for Iron in 3.5% NaCl Solutions. *ACS Omega* **2021**, *6*, 14525–14532. [CrossRef] [PubMed]
35. Sherif, E.-S.M.; Ahmed, A.H.; Abdo, H.S.; DefAllah, M.N. Impediment of iron corrosion by N,N′-bis 2-hydroxynaphthylidene amino oxamide in 3.5% NaCl solution. *Crystals* **2021**, *11*, 1263. [CrossRef]
36. Sherif, E.-S.M.; Ahmed, A.H. Alleviation of Iron Corrosion in Chloride Solution by N,N′-bis 2-Methoxynaphthylidene amino oxamide as a Corrosion Inhibitor. *Crystals* **2021**, *11*, 1516. [CrossRef]
37. Sherif, E.-S.M. Electrochemical investigations on the corrosion inhibition of aluminum by 3-amino-1,2,4-triazole-5-thiol in naturally aerated stagnant seawater. *J. Ind. Eng. Chem.* **2013**, *19*, 1884–1889. [CrossRef]
38. Sherif, E.-S.M.; Ragab, S.A.; Abdo, H.S. Role of Vanadium Additions on the Corrosion Mitigation of Ti-6Al-xV Alloy in Simulated Body Fluid. *Metals* **2020**, *10*, 903. [CrossRef]
39. Sherif, E.-S.M.; Abdo, H.S.; Alharthi, N.H. Beneficial Effects of Vanadium Additions on the Corrosion of Ti6AlxV Alloys in Chloride Solutions. *Metals* **2020**, *10*, 264. [CrossRef]
40. Sherif, E.-S.M.; Erasmus, R.M.; Comins, J.D. In situ Raman spectroscopy and electrochemical techniques for studying corrosion and corrosion inhibition of iron in sodium chloride solutions. *Electrochim. Acta* **2010**, *55*, 3657–3663. [CrossRef]
41. Sherif, E.-S.M.; Park, S.M. Inhibition of copper corrosion in 3.0% NaCl by N-phenyl-1,4-phenylenediamine. *J. Electrochem. Soc.* **2005**, *152*, 428–433. [CrossRef]